Transient response of intrinsic graphene under ultrafast interband excitation

P. N. Romanets and F. T. Vasko*
Institute of Semiconductor Physics, NAS of Ukraine, Pr. Nauky 41, Kiev 03028, Ukraine
(Received 21 November 2009; revised manuscript received 4 January 2010; published 18 February 2010)

The transient evolution of carriers in an intrinsic graphene under ultrafast excitation, which is caused by the collisionless interband transitions, is studied theoretically. The energy relaxation due to the quasielastic acoustic-phonon scattering and the interband generation-recombination transitions due to thermal radiation are analyzed. The distributions of carriers are obtained for the limiting cases when carrier-carrier scattering is negligible and when the intercarrier scattering imposes the quasiequilibrium distribution. The transient optical response (differential reflectivity and transmissivity) on a probe radiation and transient photoconductivity (response on a weak dc field) appears to be strongly dependent on the relaxation and recombination dynamics of carriers.

DOI: 10.1103/PhysRevB.81.085421 PACS number(s): 72.80.Vp, 78.67.Wj, 81.05.ue

I. INTRODUCTION

The transient response of photoexcited carriers under ultrafast interband pumping has been studied during the past decades in bulk semiconductors and heterostructures (see Ref. 1 for review). The unusual transport of carriers in graphene is caused by a neutrinolike energy spectrum in gapless semiconductor, which is described by the Weyl-Wallace model[2] and a substantial modification of scattering processes. Recently, the properties of graphene after ultrafast interband excitation attract special attention. The experimental results of relaxation dynamics of photoexcited electrons and holes were published in Refs. 3–6 for epitaxial and exfoliated graphenes, respectively. The relaxation of nonequilibrium optical phonons, which are emitted by carriers after photoexcitation, is studied in Ref. 7. The theoretical consideration of the carrier relaxation and generation-recombination processes caused by optical phonons is performed in Refs. 8 and 9. The quasielastic energy relaxation of carriers due to acoustic phonons was considered in Refs. 10 and 11 for low-energy carriers [at low temperatures or under midinfrared (IR) excitation]. In particular, an interplay between energy relaxation and generation-recombination processes determines the relaxation dynamics of photoexcited carrier distribution.[10] To the best of our knowledge, both this interplay and the relaxation dynamics at low temperatures are not considered so far. Thus, the investigation of the transient response of carriers under these conditions is timely now.

In this paper, we consider the transient response of an intrinsic graphene in the case of ultrafast interband excitation in passive region, where the carrier energies are smaller than the optical-phonon energy. Such a regime can be realized under the pumping in the mid-IR spectral region or at low temperatures, when the peak of photoexcited carriers formed immediately after the process of optical-phonon emission, remains a narrow one. Describing the photoexcitation process, we restrict ourselves by the collisionless regime, when a pulse duration τ_p is shorter than the momentum relaxation time. Considering the low-temperature transient dynamics of photoexcited carriers, one takes into account the intraband quasielastic energy relaxation due to acoustic phonons and generation-recombination interband transitions due to thermal radiation. The carrier-carrier scattering is described within the two limiting regimes: (i) when the Coulomb interaction is unessential and (ii) when intercarrier scattering imposes the quasiequilibrium distribution of carriers. With the obtained transient distribution of carriers, we analyze a time-dependent response on probe field, i.e., we consider the transient reflection and transmission in the tetrahertz and mid-IR spectral regions. The transient photoconductivity is also analyzed below because the energy relaxation corresponds to a nanosecond scale (the radiative recombination remains essential up to microsecond).

Since the electron-hole energy spectrum and scattering processes are symmetric in an intrinsic graphene, the phenomena under consideration are described by the same distribution function for electrons and holes f_{pt}. Such distribution is governed by the general kinetic equation[12,13]

$$\frac{\partial f_{pt}}{\partial t} = \sum_k J_k\{f_t|p\} + G\{f_p|t\}, \tag{1}$$

where the collision integrals $J_k\{f_t|p\}$ describe the relaxation of carriers caused by the carrier-carrier scattering ($k=cc$), the acoustic phonons ($k=ac$), and the thermal radiation ($k=r$), respectively. The photogeneration rate $G\{f_p|t\}$ describes the interband excitation of electron-hole pairs by the ultrafast pulse. Below Eq. (1) is solved with the initial condition $f_{pt\to-\infty}=f_p^{(eq)}$, where $f_p^{(eq)}$ is the equilibrium distribution. The transient response on a probe radiation is described by the dynamic conductivity due to interband transitions. The transient response on a weak dc field (photoconductivity) is considered with the use of the phenomenological model of momentum scattering suggested in Ref. 14.

The analysis carried out below is organized as follows. The photoexcitation process under the interband pumping is described in Sec. II. The transient evolution distributions are discussed in Sec. III for the cases (i) and (ii). Section IV presents a set of results of transient reflectivity and transmissivity and also the transient photoconductivity. The list of assumptions used and concluding remarks are given in the last section. In Appendixes A and B, we evaluate the inter-

 ©2010 The American Physical Society

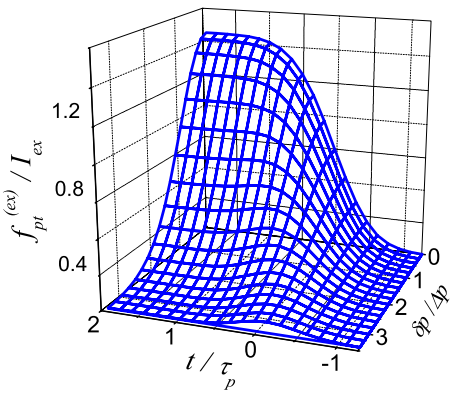

FIG. 1. (Color online) Temporal evolution of photoexcited distribution $f_{pt}^{(ex)}$ normalized to I_{ex} versus dimensionless momentum and time $\delta p/\Delta p$ and t/τ_p.

band photogeneration rate under ultrafast interband excitation and consider the dynamic conductivity.

II. ULTRAFAST EXCITATION

In the framework of the Weyl-Wallace model (spin- and valley-degenerate linear energy spectrum of carriers, which is determined by the characteristic velocity v_W), the interband photoexcitation is caused by the in-plane electric field, $w_t\mathbf{E}\exp(-i\Omega t)+\text{c.c.}$, where $\mathbf{E}$ is the field strength, Ω is the frequency, and w_t is the envelope form factor. Equation (1) is transformed to the collisionless form on the initial intervals, when the scattering mechanisms are not essential: $\partial f_{pt}/\partial t = G\{f|pt\}$. Using the boundary condition of Eq. (1), one can rewrite this equation in the integral form $f_{pt}=f_p^{(eq)} + \int_{-\infty}^{t} dt' G\{f|pt'\}$. The photogeneration rate here is evaluated in Appendixes A and B as follows:

$$G\{f_p|t\} = \left(\frac{eEv_W}{\hbar\Omega}\right)^2 w_t \int_{-\infty}^{0} d\tau w_{t+\tau} \cos\left[\left(\frac{2v_W p}{\hbar} - \Omega\right)\tau\right] \times (1-2f_{pt+\tau}), \quad (2)$$

where the Pauli blocking factor $(1-2f_{pt+\tau})$ is responsible for the coherent Rabi oscillations of the excited carriers.

Introducing the dimensionless intensity $I_{ex} = (eE\tau_p v_W/\hbar\Omega)^2$, we consider below the linear regime of excitation, which takes place if $I_{ex} \ll 1$ and $f_{pt} \ll 1$, so that the Pauli factor can be neglected [if $\hbar\Omega$ is comparable to the equilibrium temperature T, one has to use the equilibrium Pauli factor $(1-2f_p^{(eq)})$ in Eq. (2)]. Using the Gaussian form factor $w_t = \sqrt[4]{2/\pi}\exp[-(t/\tau_p)^2]$ with the pulse duration τ_p,[15] one obtains the photoexcited distribution in the form

$$f_{pt}^{(ex)} \approx \frac{I_{ex}}{\tau_p^2} \int_{-\infty}^{t} dt' w_{t'} \int_{-\infty}^{0} d\tau w_{t'+\tau} \cos\left(\frac{2v_W \delta p}{\hbar}\tau\right). \quad (3)$$

Here $\delta p = p - p_\Omega$ is centered in the characteristic momentum $p_\Omega = \hbar\Omega/2v_W$. The evolution of photoexcited distribution $f_{pt}^{(ex)}/I_{ex}$ is shown in Fig. 1. The distribution is dependent on t/τ_p and $\delta p/\Delta p$, where $\Delta p = \hbar/2v_W\tau_p$ determines the width of distribution, which is proportional to τ_p^{-1}. For $t \gg \tau_p$, the integrations in Eq. (3) can be exactly performed and we obtain the steady-state distribution after photoexcitation pulse, $f_p^{(ex)} = f_{pt\to\infty}^{(ex)}$, as the Gaussian peak of width $\propto \Delta p$

$$f_p^{(ex)} = \sqrt{\frac{\pi}{2}} I_{ex} e^{-(\delta p/\sqrt{2}\Delta p)^2}. \quad (4)$$

Thus, at $t \geq 2\tau_p$ (see Fig. 1), one can omit the photogeneration rate in Eq. (1) using instead the initial condition

$$f_{pt=0} = f_p^{(eq)} + f_p^{(ex)}, \quad (5)$$

which is given as a sum of the equilibrium and photoexcited contributions. The condition (5) can be used directly in case of weak intercarrier scattering. In case of optical excitation, with a subsequent emission of cascade of $2\mathcal{N}$ optical phonons of energy $\hbar\omega_0$, the photoexcited distribution can be written in the form (5), where δp is centered in $p_{\bar\omega} = (\hbar\Omega - 2\mathcal{N}\hbar\omega_0)/2v_W \equiv \hbar\bar\omega/2v_W$, and Δp involves an additional broadening during the cascade emission.

Under an effective intercarrier scattering, one needs to calculate the initial temperature and concentration of carriers. The photoexcited concentration and energy of carriers, which are described by the peak of distribution (4), are given by

$$\begin{vmatrix} \Delta n_{ex} \\ \Delta E_{ex} \end{vmatrix} = \frac{4}{L^2}\sum_{\mathbf{p}} \begin{vmatrix} 1 \\ v_W p \end{vmatrix} f_p^{(ex)} \simeq \frac{I_{ex}(\bar\omega/v_W)^2}{2\bar\omega\tau_p} \begin{vmatrix} 1 \\ \hbar\bar\omega/2 \end{vmatrix}, \quad (6)$$

where L^2 is the normalization area. Here one obtains $\Delta E_{ex}/n_{ex} \simeq \hbar\bar\omega/2$, for the Gaussian shape of pulse, i.e., the averaged energy per generated particle is equal to the excitation energy. In case of mid-IR excitation, we use $\mathcal{N}=0$, so that $\bar\omega \to \Omega$ in Eq. (6).

If $\tau_p \ll \tau_{cc} \ll \tau_{ac,r}$, where τ_{cc}, τ_{ac}, and τ_r correspond to the intercarrier scattering, the energy relaxation, and the generation-recombination processes, respectively [the Coulomb-controlled case (ii)], the dominating carrier-carrier scattering imposes the quasiequilibrium distribution,

$$\tilde f_{pt} = \left[\exp\left(\frac{v_W p - \mu_t}{T_t}\right) + 1\right]^{-1}, \quad (7)$$

with the effective temperature T_t and the quasichemical potential μ_t. If $\tau_{cc} \ll t \ll \tau_{ac,r}$, the initial temperature $T_{ex} = T_{t\sim 0}$ and maximal distribution $f_{ex} = f_{p=0t\sim 0}$ are determined from the concentration and energy conservation requirements

$$\frac{2}{\pi}\left(\frac{T_{ex}}{\hbar v_W}\right)^2 \int_0^\infty dx x f_x \begin{vmatrix} 1 \\ T_{ex}x \end{vmatrix} = \begin{vmatrix} n_T + \Delta n_{ex} \\ E_T + \Delta E_{ex} \end{vmatrix}, \quad (8)$$

where n_T and E_T are the equilibrium concentration and energy, and the function f_x is introduced according to $f_x \equiv f_{ex}/[e^x(1-f_{ex})+f_{ex}]$. Using Δn_{ex} and ΔE_{ex} given by Eq. (6) and solving the transcendental system (8), one obtains the initial values f_{ex} and T_{ex}. The calculations here and below are performed for the nitrogen temperature $T=77$ K, the excitation energies $2v_W p_{\bar\omega} = 120$ meV (CO_2 laser) and 60 meV (as an example of interband excitation with subsequent optical phonon emission), and the broadening energy $\hbar/\tau_p \simeq 6.6$ meV, which corresponds to the pulse duration $\simeq 0.1$ ps. In Fig. 2, we plot f_{ex} and T_{ex} versus the pumping level, which is proportional to $\Delta n_{ex}/n_T$. Fast increase of T_{ex}

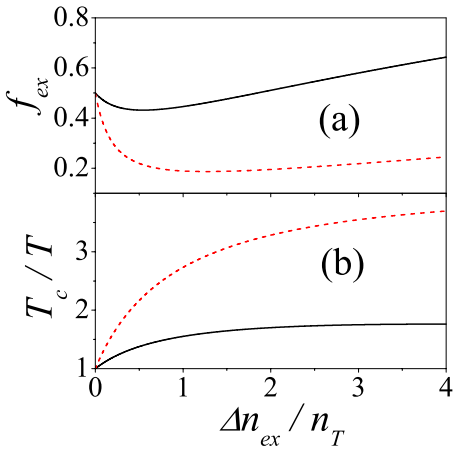

FIG. 2. (Color online) Initial maximum distribution (a) and effective temperature (b), f_{ex} and T_{ex}, versus pumping ($\Delta n_{ex}/n_T \propto I_{ex}$) for $\hbar\bar{\omega}$=60 meV and 120 meV (solid and dashed curves, respectively).

and fast decrease of f_{ex} take place for $\Delta n_{ex}/n_T < 1$, while a linear increase in these values are realized if $\Delta n_{ex}/n_T > 1$.

III. ENERGY RELAXATION AND RECOMBINATION

In this section, we analyze the transient evolution of f_{pt} caused by the energy relaxation and recombination processes. We consider the cases (i) and (ii), when the initial condition is given by Eq. (5) and written through f_{ex} and T_{ex} plotted in Fig. 2.

A. Weak intercarrier scattering

If the carrier-carrier scattering is ineffective [case (i)], the distribution f_{pt} is governed by the kinetic equation (1) without the cc contribution

$$\frac{\partial f_{pt}}{\partial t} = \frac{\nu_p^{(qe)}}{p^2}\frac{\partial}{\partial p}\left\{p^4\left[\frac{\partial f_{pt}}{\partial p} + \frac{f_{pt}(1-f_{pt})}{p_T}\right]\right\} + \nu_p^{(r)} \times [N_{2p/p_T}(1-2f_{pt}) - f_{pt}^2] \quad (9)$$

and with the initial condition (5) used instead of generation rate. Here we substituted the explicit expressions of the collision integrals for the quasielastic acoustic scattering approximation (written in the Fokker-Planck form) and for the generation-recombination processes (see discussion in Ref. 10). The Planck distribution N_{2p/p_T} is written through $p_T = T/v_W$, while the energy relaxation rate $\nu_p^{(qe)} = v_{qe}p/\hbar$ and the rate of radiative transitions $\nu_p^{(r)} = v_r p/\hbar$ are written through the characteristic velocities $v_{qe} \propto T$ and v_r.[16]

The boundary conditions are imposed by both the condition $f_{p\to\infty t}=0$, which is transformed into the requirement

$$p^4\left(\frac{\partial f_{pt}}{\partial p} + \frac{f_{pt}}{p_T}\right)_{p\to\infty} < \text{const}, \quad (10)$$

and Eq. (9) at $p=0$ which is transformed into the condition $f_{p=0t} = 1/2 + f_{p=0}^{(ex)} \exp[-(v_r/v_W)Tt/\hbar]$. According to Eq. (4), one obtains $f_{p=0}^{(ex)} = \sqrt{\pi/2} I_{ex} \exp[-(\Omega\tau_p)^2/2] \ll 1$ and one can neglect the second contribution in this condition, so that $f_{p=0t} \simeq 1/2$. Numerical solution of the Cauchy problem given by Eqs. (5), (9), and (10) is obtained below by the use of the iteration procedure.[17]

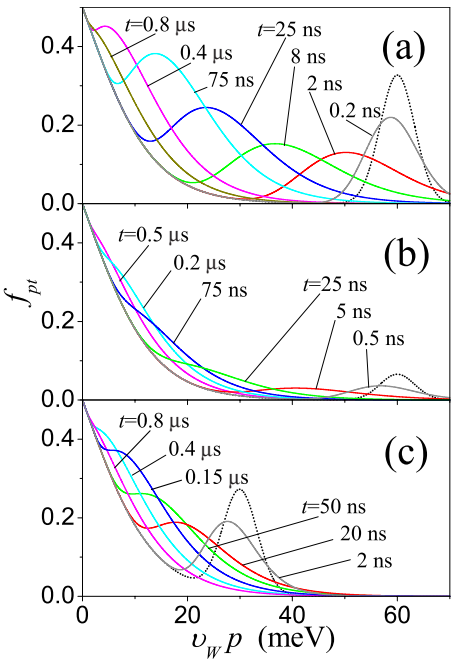

FIG. 3. (Color online) Distribution f_{pt} versus carrier energy pv_W for different delay times (marked) and excitation conditions: (a) $\hbar\bar{\omega}$=120 meV and I_{ex}=0.26, (b) $\hbar\bar{\omega}$=120 meV and I_{ex}=0.05, and (c) $\hbar\bar{\omega}$=60 meV and I_{ex}=0.21.

In Fig. 3, we demonstrate the evolution of the distribution f_{pt} at 77 K for the cases when carriers are excited around the energies 60 meV and 30 meV. The delay times are marked in panels (a)–(c) and the pumping levels are determined through the initial peak value given by $\sqrt{\pi/2} I_{ex}$ [see Eq. (4)]. Under the mid-IR pumping with pulse duration τ_p=0.1 ps and the spot sizes ~0.5 mm, the pumping levels in Figs. 3(a) and 3(b) correspond to the pulse energies ~85 pJ and ~17 pJ, respectively (see Ref. 18 for experimental details). Under optical pumping ($\hbar\Omega \sim 1.6$ eV) and subsequent emission of phonon cascade, the pumping level in Fig. 3(c) corresponds to the pulse energy ~12 nJ (duration and size are the same as above). One can see that the transient evolution of distribution occurs in two stages: energy relaxation and recombination. During the first stage [$t \lesssim 50$ ns, which is dependent on position and maximum value $f_p^{(ex)}$, see Figs. 3(a)–3(c)], the initial peak is transformed into the quasiequilibrium high-energy tail (with the equilibrium temperature caused by the energy relaxation), which is connected to the low-energy equilibrium distribution. During the next stage (up to 1 μs), the high-energy tail shifts to the lower energies and transforms into the equilibrium distribution due to effective radiative recombination in the low-energy region.

B. Coulomb-controlled case

In the carrier-carrier scattering case (ii), one has to describe the transient evolution of the effective temperature T_t

and the maximum distribution $f_t=f_{p=0t}$, which replaces the chemical potential. Since the intercarrier scattering changes neither the concentration $n_t=(4/L^2)\Sigma_{\mathbf{p}}f_{pt}$ nor the energy of carriers $E_t=(4/L^2)\Sigma_{\mathbf{p}}v_W p f_{pt}$, the balance equations for n_t and E_t take forms,[19]

$$\frac{d}{dt}\left|\begin{array}{c} n_t \\ E_t \end{array}\right| = \frac{4}{L^2}\sum_{\mathbf{p}}\left|\begin{array}{c} J_r\{\tilde{f}_t|p\} \\ v_W p[J_{ac}\{\tilde{f}_t|p\}+J_r\{\tilde{f}_t|p\}] \end{array}\right|. \quad (11)$$

Further, we transform the balance equations, expressing the left-hand side of Eq. (11) through T_t and f_t, as follows:

$$\frac{d}{dt}(T_t^2 A_t^{(1)}) = R_t^{(1)},$$

$$\frac{d}{dt}(T_t^3 A_t^{(2)}) = R_t^{(2)} + Q_t. \quad (12)$$

Here the coefficients $A_t^{(1,2)}$ are written as $A_t^{(q)}=\int_0^\infty dx x^q \tilde{f}_{xt}$, where the quasiequilibrium distribution is given by $\tilde{f}_{xt}=f_t/[e^x(1-f_t)+f_t]$, so that $A_t^{(q)}/T_t^l$ are only dependent on f_t. After substitution of the collision integral J_r (Refs. 10 and 19) and integration, the generation-recombination contributions to Eqs. (12) are obtained in the form

$$R_t^{(q)} = \frac{2v_r T_t^{q+2}}{v_W \hbar}\int_0^\infty dx x^{q+2}\tilde{f}_{xt}^2\left[\frac{e^{2x}(1-f_t)^2}{(e^{x2T_t/T}-1)f_t^2}-1\right]. \quad (13)$$

Similarly, the energy relaxation contribution is written by the use of J_{ac} as follows:

$$Q_t = \frac{T-T_t}{T}\frac{v_{qe}T_t^4}{v_W\hbar}\int_0^\infty dx x^4 e^x \tilde{f}_{xt}^2\frac{1-f_t}{f_t}. \quad (14)$$

The initial conditions for the system [Eqs. (12)] are written as $T_{t=0}=T_{ex}$ and $f_{t=0}=f_{ex}$.

Numerical solution of the nonlinear system [Eqs. (12)] is performed using the iteration procedure. In Fig. 4, we plot T_t/T and f_t versus time. Temperature relaxes to the equilibrium one during the energy relaxation times ($\lesssim$100 ns) while f_t, which is determined by the chemical potential μ_t, relaxes to 1/2 over 1 μs (the recombination time scale), in analogy with the case (i). Notice that after the fast energy relaxation, one obtains $f_t>1/2$ [dotted line in Fig. 4(b)], i.e., the low-energy electron-hole pairs appear to be unstable.[20]

Figure 5 shows the plot of temporal evolutions of the energy per particle and concentration E_t/n_t and n_t [see the definitions before Eq. (11)], for the cases (i) and (ii). The relaxation processes to the equilibrium (at nitrogen temperature, $E_{t\to\infty}/n_{t\to\infty}\simeq 14.5$ meV and $n_{t\to\infty}\simeq 5.3\times 10^9$ cm^{-2}) occur during the same scales as in Figs. 3 and 4. The temporal dependencies of n_t obtained for both cases are in good agreement (the carrier-carrier scattering does not change concentration), while E_t demonstrates a different evolution for cases (i) and (ii) at $t<50$ ns. This is because of the drift and decrease in photoexcited peak during the energy relaxation time (see Fig. 3).

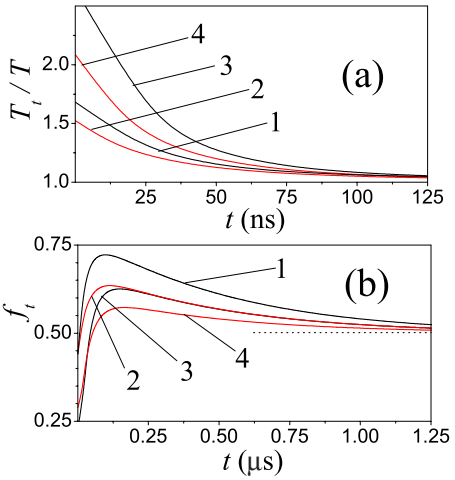

FIG. 4. (Color online) Temporal evolution of effective temperature T_t (a), and maximum distribution f_t (b), for different excitation conditions: (1) $\hbar\bar{\omega}=60$ meV and $I_{ex}=0.21$, (2) $\hbar\bar{\omega}=60$ meV and $I_{ex}=0.1$, (3) $\hbar\bar{\omega}=120$ meV and $I_{ex}=0.052$, and (4) $\hbar\bar{\omega}=120$ meV and $I_{ex}=0.026$.

IV. TRANSIENT RESPONSE

Here we turn to consideration of the response of photoexcited carriers on a probe radiation of frequency ω (reflection and transmission in the tetrahertz and mid-IR spectral regions) and on a weak dc electric field (photoconductivity). The transient electrodynamics of graphene is described using the time-dependent dynamic conductivity $\sigma_{\omega t}$, which is caused by the collisionless interband transitions (see Appendix B). The transient photoconductivity is calculated by the use of the phenomenological model of momentum relaxation suggested in Ref. 14.

A. Reflection and transmission

To calculate the transient reflectance and transmittance of the graphene sheet placed at $z=0$ on the in-plane electric

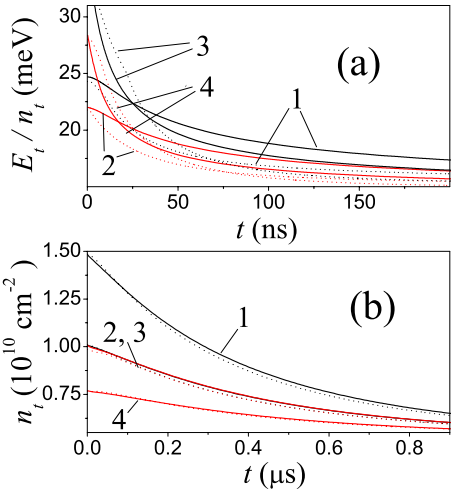

FIG. 5. (Color online) Energy per carrier (a) and concentration (b) versus time. Solid and dotted curves correspond to the cases (i) and (ii), respectively; excitation conditions (1)–(4) are the same as in Fig. 4.

field $\delta\mathbf{E}_{zt}\exp(-i\omega t)$ propagated along $0Z$, we apply the wave equation (see Ref. 21 and references therein). The induced current density $\sigma_{\omega t}\delta E_{z=0}$ is located around $z=0$ and the direction of in-plane field $\delta\mathbf{E}_{zt}$ is not essential due to the in-plane isotropy of the problem. Separating the incident radiation $E_{in}e^{ik_\omega z}$, with the wave vector $k_\omega=\omega/c$, we write the field distribution outside of the graphene sheet in the form as

$$\delta E_{zt}=\begin{cases} E_{in}e^{ik_\omega z}+E_t^{(r)}e^{-ik_\omega z}, & z<-0 \\ E_t^{(t)}e^{i\bar{k}_\omega z}, & z>+0 \end{cases}, \tag{15}$$

where $\bar{k}_\omega=\sqrt{\epsilon}\omega/c$ is the wave vector in the substrate with the dielectric permittivity ϵ. The transmitted and reflected electric fields $E_t^{(t)}$ and $E_t^{(r)}$ are determined from the boundary conditions at $z\to 0$ as follows:

$$\frac{E_t^{(t)}}{E_{in}}=\frac{2}{1+A_{\omega t}}, \quad \frac{E_t^{(r)}}{E_{in}}=\frac{1-A_{\omega t}}{1+A_{\omega t}}. \tag{16}$$

Here we introduce the dimensionless factor $A_{\omega t}=\sqrt{\epsilon}+(4\pi/c)\sigma_{\omega t}$. The reflection and transmission coefficients $R_{\omega t}=|E_t^{(r)}|^2/E_{in}^2$ and $T_{\omega t}=\sqrt{\epsilon}|E_t^{(t)}|^2/E_{in}^2$ are written through $A_{\omega t}$, according to

$$R_{\omega t}=\left|\frac{1-A_{\omega t}}{1+A_{\omega t}}\right|^2, \quad T_{\omega t}=\frac{4\sqrt{\epsilon}}{|1+A_{\omega t}|^2}. \tag{17}$$

Using $\sigma_{\omega t}$ determined by Eqs. (B3), we consider below the differential changes in reflectivity and transmissivity $(\Delta R/R)_{\omega t}=(R_\omega^{(eq)}-R_{\omega t})/R_\omega^{(eq)}$ and $(\Delta T/T)_{\omega t}=(T_\omega^{(eq)}-T_{\omega t})/T_\omega^{(eq)}$, which are written through the equilibrium reflection and transmission coefficients $R_\omega^{(eq)}$ and $T_\omega^{(eq)}$.

The evolution of the differential reflectivity for the cases (i) and (ii) is shown in Figs. 6(a)–6(c), respectively. If the Coulomb scattering is not effective [case (i)], the distribution of photoexcited carriers relaxes during the energy relaxation time scale (around 10 ns, cf. with Fig. 3), when a quenching of peak takes place (if $\hbar\omega$ is comparable with the peak energy). In case (ii), any peculiarities of the spectral dependencies at short times are absent because the initial distribution is transformed into the quasiequilibrium one during times $\sim\tau_{cc}\to 0$. The further evolution of $(\Delta R/R)_{\omega t}$ is limited by the generation-recombination process and extended up to microseconds. In the tetrahertz spectral region ($\hbar\omega\geq 10$ meV is considered here because we neglect the intraband relaxation), the differential reflectivity increases and changes a sign. In the high-energy region, $(\Delta R/R)_{\omega t}$ decreases monotonically with ω and t and does not exceed $\sim 10^{-4}$ for the near-IR spectral region. Besides, the response is approximately proportional to the pumping intensity I_{ex}, and $(\Delta R/R)_{\omega t}$ increases with increasing of the photoexcitation energy $\hbar\bar{\omega}$ [cf. Figs. 6(b) and 6(c)].

In Fig. 7, we plot the differential transmissivity for the cases (i) and (ii) under the same excitation conditions. Once again, in the high-frequency region, the differential transmissivity decreases slowly (during a microsecond time scale) and $(\Delta T/T)_{\omega t}$ does not exceed $\sim 10^{-4}$ for the near-IR spectral region. In the tetrahertz spectral region, $(\Delta T/T)_{\omega t}$ increases and changes the sign in the same manner as $(\Delta R/R)_{\omega t}$ (cf. Figs. 6 and 7). The dependencies on the excitation parameters (I_{ex} and $\hbar\bar{\omega}$) are also similar to the reflectivity. Additionally, in case (i), a fast (at $t<10$ ns) quenching of the photoexcited peak contribution in the spectral region $\sim\hbar\Omega$ takes place.

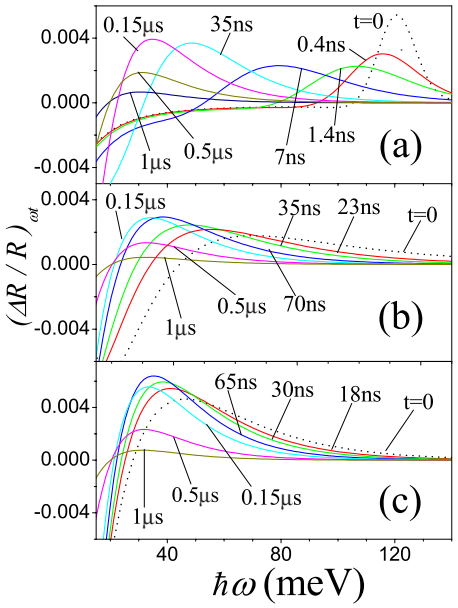

FIG. 6. (Color online) (a) Spectral dependencies of differential reflectivity $(\Delta R/R)_{\omega t}$, for different delays (marked) at the excitation conditions: (a) $\hbar\bar{\omega}=120$ meV and $I_{ex}=0.052$ in the case (i), (b) $\hbar\bar{\omega}=120$ meV and $I_{ex}=0.052$ in the case (ii), and (c) $\hbar\bar{\omega}=60$ meV and $I_{ex}=0.21$ in the case (ii).

B. Photoconductivity

Finally, we consider the transient photoconductivity, i.e., the response of photoexcited carriers to a weak dc electric field. Since the momentum relaxation is governed by a fast elastic scattering,[14] one can use the dc conductivity σ_t, which depends on time through f_{pt}

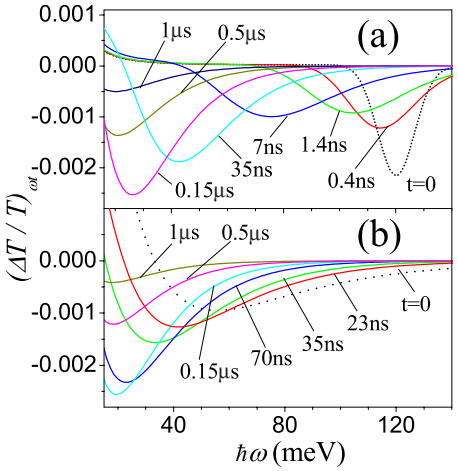

FIG. 7. (Color online) (a) Differential transmissivity $(\Delta T/T)_{\omega t}$ versus $\hbar\omega$ and t for cases (i) and (ii) [panels (a) and (b), respectively] at the same excitation conditions: $\hbar\bar{\omega}=120$ meV, $I_{ex}=0.052$.

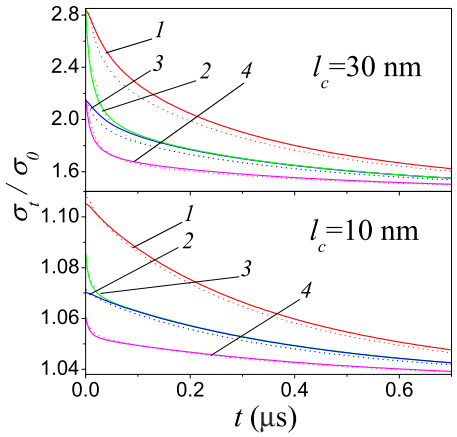

FIG. 8. (Color online) Temporal evolution of conductivity for excitation conditions (1)–(4), which are the same as in Fig. 4 for the correlation length l_c=30 and 10 nm. Solid and dashed curves are correspondent to the cases (ii) and (i).

$$\sigma_t = \sigma_0 \left[2f_{p=0t} - \frac{l_c}{\hbar} \int_0^\infty dp f_{pt} \frac{\Psi'(pl_c/\hbar)}{\Psi(pl_c/\hbar)^2} \right]. \quad (18)$$

Here l_c is the correlation length, characterizing the disorder scattering, and the function $\Psi(z)=e^{-z^2}I_1(z^2)/z^2$ is written through the first-order Bessel function of imaginary argument $I_1(z)$. The normalized conductivity σ_0 is introduced for the case of short-range scattering, when $l_c=0$. The distribution $f_{p=0t}$ is shown in Fig. 4(b) for the case (ii) while $2f_{p=0t}=1$ for the case (i). If $l_c=0$, one obtains $\sigma_t/\sigma_0=1$, i.e., there is no transient photoconductivity for the case (i); for the case (ii), one obtains $\sigma_t/\sigma_0=2f_t$ and the transient photoconductivity is clear from Fig. 4(b).

For the finite-range momentum scattering case, if $l_c \neq 0$, the transient evolution of conductivity is shown in Fig. 8. For the definiteness, it was assumed that l_c=10 and 30 nm and variations of σ_t are increased with l_c essentially due to contribution of high-energy carriers. Similar to Sec. IV A, one can separate two stages of evolution: the fast decrease of σ_t due to energy relaxation (up to ~30–50 ns for the conditions considered) and the slow quenching of σ_t due to carrier recombination. If $t>1$ μs, the conductivity approaches to the equilibrium values: $\sigma_{t\to\infty}/\sigma_0=1.445$ if l_c=30 nm and $\sigma_{t\to\infty}/\sigma_0=1.035$ if l_c=10 nm. Since the transient conductivity can be measured for the subnanosecond time scale,[22] such a scheme can be used for verification of both energy relaxation and recombination mechanisms.

V. CONCLUDING REMARKS

To summarize, we have considered both the interband ultrafast photoexcitation and the relaxation dynamics of the carriers in an intrinsic graphene. In contrast to the measurements[3–6] and calculations[8,9] performed, where the evolution corresponds to the subpicosecond time scales due to the optical-phonon contribution, here we consider the slow relaxation of the low-energy carriers. The distribution of carriers at T=77 K is obtained for the limiting cases with negligible or dominating intercarrier scattering when the energy relaxation and generation-recombination processes are caused by the quasielastic acoustic-phonon scattering and thermal radiation, respectively. The initial distribution is obtained in the framework of the linear, with respect to pumping, approximation for the collisionless regime of the interband transitions. The transient optical response on the probe radiation (transmission and reflection) as well as on the weak dc field (transient photoconductivity) appears to be strongly dependent on the relaxation and recombination dynamics of carriers.

Next, we discuss the assumptions made. The main restrictions of the results presented are the consideration of the low-energy carriers, when the interaction with optical phonons is unessential, and the single generation-recombination mechanism (due to thermal radiation) is taken into account. These conditions are realized at low temperatures under the mid-IR ultrafast excitation[18] of the clean sample (e.g., suspended graphene[23]). Such an approach can be used for the case of optical interband excitation, when the low-energy initial distribution, with a phenomenological broadening, is formed after the cascade process of optical-phonon emission. The consideration is restricted by the radiative recombination case (the Auger processes are forbidden due to the symmetry of electron-hole states[24]), with the characteristic time scales up to microseconds. Any visible contribution of other generation-recombination mechanism (e.g., because of disorder-induced interband transitions with acoustic phonons, or under intercarrier scattering) leads to a fast decrease in photoresponse. Such a regime requires an additional investigation, but the quasielastic energy relaxation stage (time scales up to 50 ns at T=77 K) is described by the presented results.

The rest of assumptions are rather standard. The consideration in Sec. III is limited by the simple cases (i) and (ii), with and without the intercarrier scattering. The main peculiarities of the response under consideration are similar for both cases, but the complete description of the nonequilibrium carriers had been performed neither under optical excitation nor under high dc field (see Refs. 19 and 25 and references therein). The description of the momentum relaxation in Sec. IV is based on the phenomenological model of Ref. 13. The utilization of the quasielastic energy scattering and the collisionless interband photoexcitation appear to be rather natural. The listed assumptions do not change either the character of the response or the numerical estimates.

In closing, the peculiarities of the transient optical response (transmission and reflection) as well as of the transient photoconductivity appear to be useful tools in order to verify the relaxation and generation-recombination mechanisms of carriers. Thus, in addition to the recently obtained experimental results,[3–7] measurements under mid-IR excitation and at low temperature will be useful for characterization of graphene.

APPENDIX A: GENERATION RATE

Below we describe the interband carrier excitation under ultrafast mid-IR pumping $\mathbf{E}_t \exp(-i\Omega t)+$c.c. for the colli-

sionless case, when τ_p is shorter than relaxation times. The photogeneration rate into the α state is determined by the general expression (see Ref. 1 and Sec. 54 in Ref. 12)

$$G_{\alpha t} = 2\,\mathrm{Re}\left(\frac{e}{\hbar\Omega}\right)^2 \int_{-\infty}^{0} d\tau e^{\lambda\tau - i\Omega\tau} \times \langle\alpha|[e^{i\hat{h}\tau/\hbar}[(\mathbf{E}_{t+\tau}\cdot\hat{\mathbf{v}}),\hat{\rho}_{t+\tau}]e^{-i\hat{h}\tau/\hbar},(\mathbf{E}_t\cdot\hat{\mathbf{v}})^+]|\alpha\rangle, \tag{A1}$$

where $\hat{\rho}_t$ is the density matrix, $\hat{\mathbf{v}}$ is the velocity operator, and $\lambda \to +0$. Since the collisionless regime of photoexcitation, we calculate Eq. (A1) with the use of the free states $|l\mathbf{p}\rangle$ and the energy ε_{lp}, where $l = \pm 1$ stands for c or v bands and $\mathbf{p}$ is the two-dimensional momentum. Neglecting the nondiagonal components of the density matrix $\hat{\rho}_t$ and using the distribution functions $f_{l\mathbf{p}t}$, one obtains the generation rate

$$G\{f_{\mathbf{p}}|1t\} = \left(\frac{e}{\hbar\Omega}\right)^2 \int_{-\infty}^{0} d\tau e^{\lambda\tau - i\Omega\tau} e^{i(\varepsilon_{1p}-\varepsilon_{-1p})\tau/\hbar} \times \langle 1\mathbf{p}|(\mathbf{E}_{t+\tau}\cdot\hat{\mathbf{v}})|-1\mathbf{p}\rangle\langle -1\mathbf{p}|(\mathbf{E}_t\cdot\hat{\mathbf{v}})^+|1\mathbf{p}\rangle \times (f_{-1\mathbf{p}t+\tau} - f_{1\mathbf{p}t+\tau}) + \mathrm{c.c.}, \tag{A2}$$

moreover, $G\{f_{\mathbf{p}}|-1t\} = -G\{f_{\mathbf{p}}|1t\}$, according to the particle conservation law. Next, we separate the envelope form factor w_t using $\mathbf{E}_t = \mathbf{E}w_t$ and take into account the in-plane isotropy of the problem, when one arrives to the averaged matrix element $\overline{|\langle +1\mathbf{p}|(\mathbf{E}\cdot\hat{\mathbf{v}})|-1\mathbf{p}\rangle|^2} = (Ev_W)^2/2$. As a result, we obtain the in-plane isotropic generation rate $G\{f_p|t\} = \pm G\{f_p|\pm 1t\}$ in the following form:

$$G\{f_p|t\} = \left(\frac{eEv_W}{\hbar\Omega}\right)^2 \frac{w_t}{2} \int_{-\infty}^{0} d\tau w_{t+\tau} e^{\lambda\tau - i\Omega\tau} e^{i(2v_W p)\tau/\hbar} \times (f_{-1pt+\tau} - f_{1pt+\tau}) + \mathrm{c.c.} \tag{A3}$$

Finally, using the electron-hole representation[19] and replacing the filling factor here by $(1-2f_{pt})$, we arrive at Eq. (2).

APPENDIX B: DYNAMIC CONDUCTIVITY

The response of graphene on the in-plane probe field $\delta\mathbf{E}\exp(-i\omega t)$ is described by the dynamic conductivity[21,26]

$$\sigma_{\omega t} \approx i\frac{2(ev_W)^2}{\omega L^2}\sum_{\mathbf{p}}(1-2f_{pt}) \times \left(\frac{1}{\hbar\omega - 2v_W p + i\lambda} - \frac{1}{\hbar\omega + 2v_W p + i\lambda}\right), \tag{B1}$$

with $\lambda \to +0$. The parametric time dependency of $\sigma_{\omega t}$ is valid because the time scales under consideration exceed ω^{-1}. It is convenient to separate the time-independent contribution $\bar{\sigma}_\omega$ described the undoped graphene in the absence of photoexcitation, when f_{pt} vanishes. Using the energy conservation law, one obtains $\mathrm{Re}\,\bar{\sigma}_\omega = e^2/4\hbar$. In the framework of the Weyl-Wallace model, the imaginary contribution into $\bar{\sigma}_\omega$ appears to be divergent at $p \to \infty$.[27] It is convenient to approximate $\mathrm{Im}\,\bar{\sigma}_\omega$ as a sum of $\propto\omega^{-1}$ and $\propto\omega$ terms, which correspond to the contributions of the virtual interband transitions and the ion background, correspondingly. As a result, we obtain

$$\mathrm{Im}\,\bar{\sigma}_\omega \approx \frac{e^2}{\hbar}\left(\frac{\varepsilon_m}{\hbar\omega} - \frac{\hbar\omega}{\varepsilon_i}\right), \tag{B2}$$

where the characteristic energies $\varepsilon_m \simeq 0.1$ eV, and $\varepsilon_i \simeq 6.8$ eV are correspondent to the recent measurements of the graphene optical spectrum.[21,28]

Next, substituting the time-dependent distribution f_{pt} obtained in Sec. III into the dynamic conductivity (B1), one transforms the real and imaginary parts of $\sigma_{\omega t}$ as follows:

$$\mathrm{Re}\,\sigma_{\omega t} = \frac{e^2}{4\hbar}[1 - 2F_{p_\omega,t}],$$

$$\mathrm{Im}\,\sigma_{\omega t} = \mathrm{Im}\,\bar{\sigma}_\omega - \frac{e^2}{\pi\hbar}\mathcal{P}\int_0^\infty \frac{dyy^2}{1-y^2}F_{p_\omega y,t}. \tag{B3}$$

Here $\mathcal{P}$ means the principal value of integral. We also introduced the function $F_{p,t} = f_{pt}$ for the case (i) and $F_{p,t} = \tilde{f}_{pt}$ for the case (ii), when $\sigma_{\omega t}$ is determined both the effective temperature and the carrier concentration T_t and f_t.

*ftvasko@yahoo.com

[1] J. Shah, *Ultrafast Spectroscopy of Semiconductors and Semiconductor Nanostructures* (Springer, New York, 1996); F. T. Vasko and A. V. Kuznetsov, *Electron States and Optical Transitions in Semiconductor Heterostructures* (Springer, New York, 1998).

[2] E. M. Lifshitz, L. P. Pitaevskii, and V. B. Berestetskii, *Quantum Electrodynamics* (Butterworth-Heinemann, Oxford, 1982); P. R. Wallace, Phys. Rev. **71**, 622 (1947).

[3] J. M. Dawlaty, S. Shivaraman, M. Chandrashekhar, F. Rana, and M. G. Spencer, Appl. Phys. Lett. **92**, 042116 (2008).

[4] D. Sun, Z.-K. Wu, C. Divin, X. Li, C. Berger, W. A. de Heer, P. N. First, and T. B. Norris, Phys. Rev. Lett. **101**, 157402 (2008).

[5] P. A. George, J. Strait, J. Dawlaty, S. Shivaraman, Mvs. Chandrashekhar, F. Rana, and M. G. Spencer, Nano Lett. **8**, 4248 (2008).

[6] R. W. Newson, J. Dean, B. Schmidt, and H. M. van Driel, Opt. Express **17**, 2326 (2009).

[7] H. Wang, J. Strait, P. George, S. Shivaraman, V. Shields, M. Chandrashekhar, J. Hwang, C. Ruiz-Vargas, F. Rana, M. Spencer, and J. Park, arXiv:0909.4912 (unpublished).

[8] S. Butscher, F. Milde, M. Hirtschulz, E. Malic, and A. Knorr, Appl. Phys. Lett. **91**, 203103 (2007).

[9] F. Rana, P. A. George, J. H. Strait, J. Dawlaty, S. Shivaraman, Mvs. Chandrashekhar, and M. G. Spencer, Phys. Rev. B **79**,

115447 (2009).
[10] F. T. Vasko and V. Ryzhii, Phys. Rev. B **77**, 195433 (2008); A. Satou, F. T. Vasko, and V. Ryzhii, *ibid.* **78**, 115431 (2008).
[11] R. Bistritzer and A. H. MacDonald, Phys. Rev. Lett. **102**, 206410 (2009).
[12] F. T. Vasko and O. E. Raichev, *Quantum Kinetic Theory and Applications* (Springer, New York, 2005).
[13] In general case, $J_k\{f_t|p\}$ and $G\{f_p|t\}$ are nonlocal operators with respect to p and t variables. The calculations here are based on the local approaches.
[14] F. T. Vasko and V. Ryzhii, Phys. Rev. B **76**, 233404 (2007).
[15] The form factor w_t is normalized according to the condition $\int_{-\infty}^{\infty} dt w_t^2 = \tau_p$. The shape of normalized form factor has little effect on the transient photoexcitation under consideration because the ultrafast response is determined fundamentally by the pulse duration τ_p.
[16] Here we use the characteristic velocities $v_{ac} \simeq 2.5 \times 10^5$ cm/s (for the nitrogen temperature) and $v_r \simeq 41.6$ cm/s (for graphene sheet placed between SiO_2 substrate and cover layer) (see Ref. 10).
[17] D. Potter, *Computational Physics* (John Wiley, London, 1973).
[18] T. Elsaesser and M. Woerner, Phys. Rep. **321**, 253 (1999).
[19] O. G. Balev, F. T. Vasko, and V. Ryzhii, Phys. Rev. B **79**, 165432 (2009).
[20] According to Eq. (B3), the negative interband absorption ($\propto \mathrm{Re}\ \sigma_{\omega t}$) takes place, if $f_{pt} > 1/2$ (see Ref. 10 and references therein). This low-energy instability is suppressed due to an effective intraband (Drude) absorption.
[21] L. A. Falkovsky, Phys. Usp. **51**, 887 (2008); T. Stauber, N. M. R. Peres, and A. K. Geim, Phys. Rev. B **78**, 085432 (2008); M. V. Strikha and F. T. Vasko, *ibid.* (to be published).
[22] T. Yao, K. Inagaki, and S. Maekawa, *Proceedings of the 11th International Conference on the Physics of Semiconductors* (Polish Scientific, Warszawa, 1972), Vol. 1, p. 417.
[23] G. Li, A. Luican, and E. Y. Andrei, Phys. Rev. Lett. **102**, 176804 (2009); P. Neugebauer, M. Orlita, C. Faugeras, A. L. Barra, and M. Potemski, *ibid.* **103**, 136403 (2009).
[24] M. S. Foster and I. L. Aleiner, Phys. Rev. B **79**, 085415 (2009).
[25] A. Akturk and N. Goldsman, J. Appl. Phys. **103**, 053702 (2008); R. S. Shishir and D. K. Ferry, J. Phys.: Condens. Matter **21**, 344201 (2009).
[26] R. R. Nair, P. Blake, A. N. Grigorenko, K. S. Novoselov, T. J. Booth, T. Stauber, N. M. R. Peres, and A. K. Geim, Science **320**, 1308 (2008); K. F. Mak, M. Y. Sfeir, Y. Wu, C. H. Lui, J. A. Misewich, and T. F. Heinz, Phys. Rev. Lett. **101**, 196405 (2008).
[27] A. Principi, M. Polini, and G. Vignale, Phys. Rev. B **80**, 075418 (2009).
[28] M. Bruna and S. Borini, Appl. Phys. Lett. **94**, 031901 (2009).